6 The electron transfer chain

6.1 Introduction

The function of the ETC is the charge separation and the stabilisation of two radical species. The ETC is embedded in the RC formed by D1 and D2 and isolated from the protein matrix of other subunits. This spatial separation protects the protein surrounding from the highly reactive radicals formed during the photosynthetic cycle and reduces possible energy-wasting side reactions. This increases the efficiency and the quantum yield, which is *in vivo* close to one.

Different cofactors are involved in electron transfer, and their properties are optimised for efficient electron transfer. The distance, orientation and midpoint potentials of neighbouring cofactors are modulated such that reduction of the following cofactor along the ETC occurs much faster than the back reaction (oxidation or charge recombination), if the electron is transferred to the oxidised primary electron donor $P680^{*+}$. The redox potential of each cofactor is not only limited by its chemical properties, but also significantly influenced by the protein surrounding. For PbRC numerous mutants are reported that modulate the redox properties of the nearby cofactors e.g. (Bylina *et al.*, 1988; Allen *et al.*, 1996).

All cofactors of the ETC are embedded in the RC subunits D1 and D2, resembling the arrangement of the ETC in PSI (C-terminal domains of PsaA and PsaB) and of the ETC in PbRC (L and M subunits). From the lumen to the cytoplasm the cofactors are as follows: Mn-Ca-cluster, Tyr_Z and Tyr_D, P_{D1}, P_{D2}, Chl_{D1}, Chl_{D2}, $Chlz_{D1}$, $Chlz_{D2}$, $Pheo_{D1}$, $Pheo_{D2}$, Q_A, non-haem Fe^{2+} and Q_B (Fig. 6.1). Except for the Mn-Ca-cluster, the cofactors of the ETC are arranged in two branches related by the local pseudo-$C2$(Fe^{2+}) axis (Fig. 6.1), as in PbRC (Deisenhofer *et al.*, 1995) and PSI (Jordan *et al.*, 2001). Their side chains are well defined in the electron density except for Q_A that could only be modelled as benzene, and the mobile Q_B was probably lost during isolation and preparation. Although the arrangement and orientation of the cofactors constituting the two branches of the ETC are similar in PSIIcc and PbRC (Deisenhofer *et al.*, 1995), there are some notable differences. The symmetric arrangement is reflected in nearly equal distances between corresponding cofactors of each branch (Fig. 6.1).

The electron transfer chain

It is difficult to relate spectroscopically identified individual cofactors to certain cofactors in the structure. This is due the impossibility to determine the spectroscopic properties of one single structural element (D1, D2, CP47, CP43) isolated from the others. Another problem is the insufficient resolution of the current model. At this stage it is difficult to discuss e.g. H-bonding. Another important point to mention is that water molecules are not modelled. Such water molecules could for instance coordinate Chl$a$ or mediate H-bonds to cofactors.
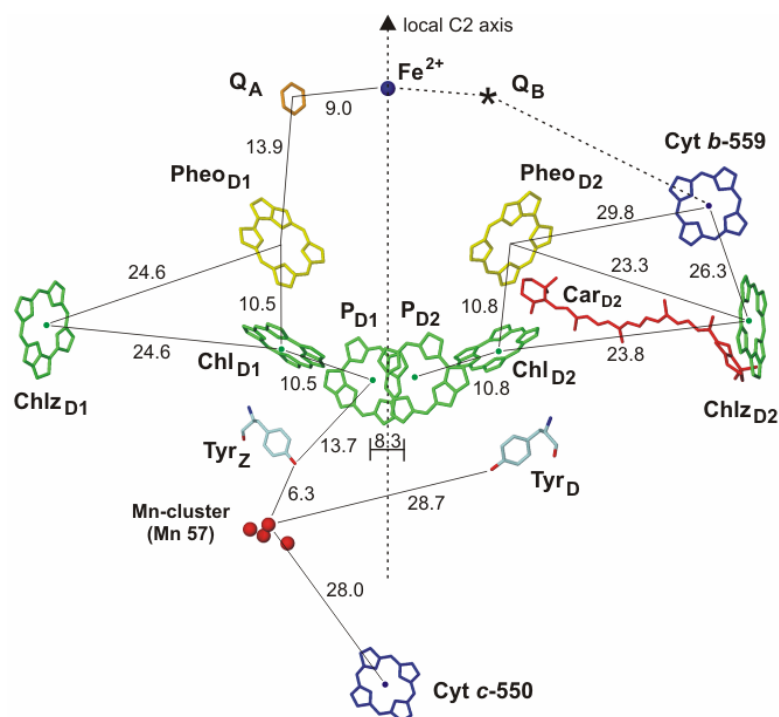

Fig. 6.1: View of the ETC along membrane plane. Chl$a$ (green), Pheo$a$ (yellow), haem (blue) represented schematically without side chains, putative Q_B site marked by asterisk. Car and Mn-Ca-cluster are drawn in red. Distances are given in Å.

6.2   Cofactors of the ETC

6.2.1   The special pair - P680

From the analogy with PbRC, D1-His198 and D2-His197 were proposed to coordinate the two Chl$a$ of P680 (Trebst, 1986; Michel and Deisenhofer, 1988). The chlorophylls, named P_{D1} and P_{D2} are orientated nearly perpendicular to the membrane (Table 10.3). In first structural model the centre-to-centre distance was about 10 Å (Zouni $et\ al.$, 2001). Further refinement revealed a distance of 8.7 Å (Vasil'ev $et\ al.$, 2001). In the 3.2 Å structure, Chl$a$ P_{D1} is coordinated by D1-His198Nϵ and P_{D2} by D2-His197Nϵ (Table 10.1); the distance between

the two Mg^{2+} ions is 8.3 Å and the interplanar separation of the chlorin heterocycles is 3.4 Å. The environment of P_{D1} and P_{D2} is mainly hydrophobic (Table 6.1 and Table 10.3) with no evidence for direct H-bonding to protein. Four Phe (D1-Phe169, D1-Phe184, D1-Phe185, D1-Phe188) located on helix **cd** of D2 form a hydrophobic floor proximal to P680. D2-Arg180, located in the neighbourhood of P_{D2}, was suggested to contribute an up-shift of the electrochemical potential of P680 (Manna *et al.*, 1998; Mulkidjanian, 1999). The proximity between the guanidinium head group of D2-Arg180 and P_{D2} (edge-to-edge distance ~8 Å) might be responsible for the higher potential of P_{D2}. The corresponding counterpart is D1-Asn181 (edge-to-edge distance ~17 Å) seems to have only a marginal influence on P680.

Table 6.1: Protein environment of selected cofactors within the ETC.

P_{D1}	P_{D2}	Chl_{D1}	Chl_{D2}	$Pheo_{D1}$	$Pheo_{D2}$
D1-Met183*	D2-Leu 182*	D1-Phe119	D2-Gly118	D1-Tyr126[†]	D2-Phe125
D1-Phe 186	D2-Phe185	D1-Val157	D2-Val156	D1-Gln130[†]	D2-Gln129
D1-Gln187	D2-Gln186[†]	D1-Phe158	D2-Phe157	D1-Ile143	D2-Asn142
D1-Ile192	D2-Trp191	D1-Met172	D2-Pro171	D1-Tyr147[†]	D2-Phe146
D1-Val202	D2-Val201	D1-Ile176	D2-Val175	D1-Pro150	D2-Pro149
D1-Val205	D2-Val204	D1-Thr179	D2-Ile178	D1-Val283	D1-Phe206
D1-Phe 206*	D2-Leu 205*	D1-Phe180	D2-Phe179	D2-Leu209	D1-Leu210
D1-Leu279*	D2-Ser282	D1-Phe182	D2-Phe181	D2-Ala212	D1-Ala213
D1-Thr286	D2-Leu283*	D1-Met183	D2-Leu182	D2-Ile213	D1-Met214
D1-Ile290	D2-Val 286	D2-Met198	D1-Gln199[†]	D2-Phe257	D1-Ile259
		D2-Val201	D1-Val202	D2-Leu205	D2-Leu279
		D2-Leu205	D1-Phe206		

$Chlz_{D1}$	$Chlz_{D2}$	Tyr_Z	Tyr_D	Q_A	Q_B
D1-Ile36	D2-Leu36	D1-Tyr161	D2-Tyr160	D2-His214	D1-Phe211
D1-Pro39	D2-Pro39	D1-Pro162	D2-Pro161	D2-Thr217	D1-Met214
D1-Thr40	D2-Cys40	D1-Ile163	D2-Gly163	D2-Met 246	D1-His215
D1-Ala43	D2-Leu43	D1-Gln165[†]	D2-Gln164[†]	D2-Trp253	D1-Leu218
D1-Pro95	D2-Leu91	D1-Phe182	D2-Phe181	D2-Ala260	D1-Ala251
D1-Ile96	D2-Thr112	D1-Phe186	D2-Phe184	D2-Phe261	D1-Phe255
D1-Leu114	D2-Phe113	D1-Glu189[†]	D2-Phe185	D2-Leu267	D1-Ile259
D1-Leu121	D2-Phe120	D1-His190[†]	D2-Phe188		D1-Leu271
TMH 1	TMH 8		D2-His189[†]		D1-Phe274

* residues contributing simultaneously to the binding pockets of P_{D1} and P_{D2}

[†] forming H-bond to cofactor

The electron transfer chain

D2-Trp191, shown to be important for the high redox potential of P680$^{+\bullet}$ (Keilty *et al.*, 2001), stacks with D2-His197 and is in van der Waals contact with P_{D2}. ENDOR and EPR studies showed that the formed cation radical P680$^{+\bullet}$ is localised on a monomeric Chl*a* (Rigby *et al.*, 1994) identified as P_{D1} by spectroscopic studies on D1-His198 mutants (Diner *et al.*, 2001). Determination of the distance between P680$^{+\bullet}$ and $Q_A^{-\bullet}$ by EPR experiments, showed a distance of 27.7 Å (Zech *et al.*, 1997; Zech *et al.*, 1999). This is in good agreement with the distance between $Q_A^{-\bullet}$ and $P_{D1}^{+\bullet}$ (27.9 Å) and P_{D2} (28.3 Å) taking the coordinate error in account (Table 10.2). The distance between $Q_A^{-\bullet}$ and the accessory Chla_{D1} and Chla_{D2} are either too short or too long. From these findings we conclude that P_{D1} is the most probable candidate for P680$^{+\bullet}$.

Spectroscopic studies of P_{D1}, P_{D2}, Chl$_{D1}$ and Chl$_{D2}$ are hampered by strong coupling between their four chlorin rings. Consequently there might be almost no spectral separation between them resulting in largely overlapping absorption bands between 670 and 680 nm. In addition excitation energy could be transferred from the antenna system to each of the porphyrins.
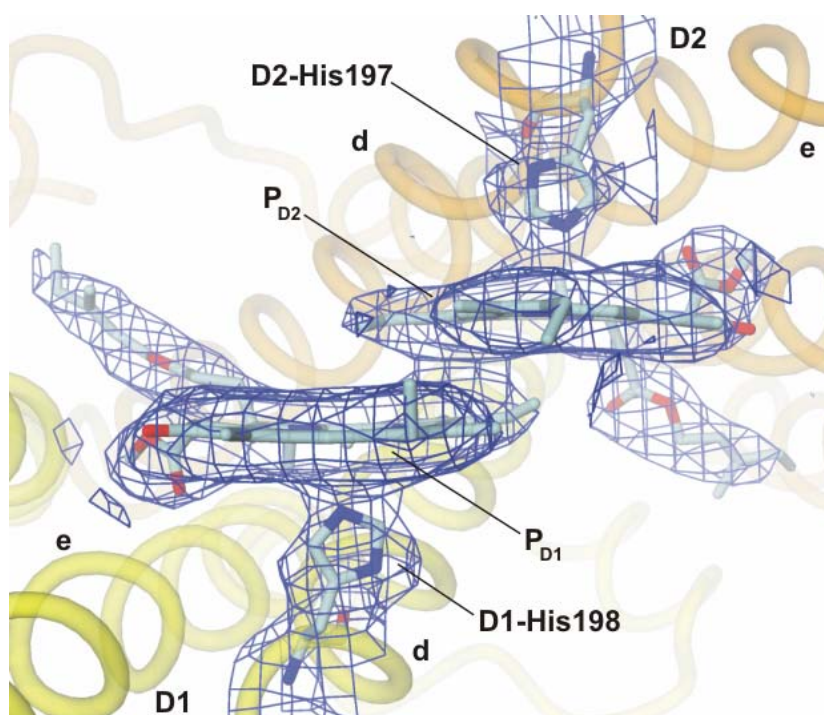

Fig. 6.2: Coordination and environment of the primary electron donor. P_{D1} is coordinated by D1-His198 and its counterpart P_{D2} by D2-His197. Both cofactors are embedded within TMH-**d** and -**e** of D1 (yellow) and D2 (orange), respectively. Electron density (blue) is contoured at 1.2 σ level. Side chains and phytol chains of the Chl*a* are clearly defined in the electron density.

Although the arrangement and orientation of the cofactors constituting the two branches of the ETC are similar in PSIIcc and PbRC, there are some notable differences. The $Mg^{2+} \cdots Mg^{2+}$ distance of P_{D1}/P_{D2} in PSIIcc, 8.3 Å, is only 0.7 Å longer than that of the two bacteriochlorophyll b of P960, 7.6 Å (Deisenhofer $et\ al.$, 1995), suggesting that P680 could likewise act as a special Chl$a$ pair. Contradictory to the special pair model is that the observed excitonic coupling between P_{D1} and P_{D2} is much smaller than expected and led to the multimer model (Tetenkin $et\ al.$, 1989; Hillmann $et\ al.$, 1995). However, according to the multimer model, the excited singlet state $^1P680^*$ is delocalised over all four Chl$a$ (P_{D1}, P_{D2}, Chl_{D1}, Chl_{D2}), and possibly includes the two Pheo$a$. They act as a collective state, thereby promoting fast and efficient charge separation (Peterman $et\ al.$, 1998; Barter $et\ al.$, 2003). Optical spectroscopy on partially orientated samples suggested that the triplet state $^3P680$ is located on a Chl$a$ molecule tilted by 30° to the membrane plane (van Mieghem $et\ al.$, 1991). Chl_{D1} and Chl_{D2} fulfil this geometric requirement but not P_{D1} or P_{D2} (Table 10.3). An increased distance between P_{D1} and P_{D2} also reduces electronic coupling, which in turn probably contributes to the higher midpoint redox potential for the primary donor in PSII compared to PbRC (1.17 V in $P680^{+\bullet}/P680$ $versus$ 0.52 V in $P960^{+\bullet}/P960$) (Adam and Ostersetzer, 2001; Barber and Archer, 2001), finally allowing electron abstraction from Tyr_Z and the Mn-Ca-cluster. The environment of P_{D1}/P_{D2} is more hydrophobic than that of P960 in PbRC, where three H-bonds have been identified (Deisenhofer $et\ al.$, 1995). Strong H-bonding may increase the redox potential, but in PSIIcc only one H-bond is found for Chl_{D2} (D1-Glu199Nε2; 3.5 Å), and none to the accessory bacteriochlorophyll b in PbRC. These differences are likely to influence the redox potential of P680.

Several factors may increase the redox potential of a Chl$a$: (i) protonation of the keto-group, which is not determinable at 3.2 Å resolution, (ii) unusual coordination of the central Mg^{2+} atom and (iii) a strong electrical field in the binding pocket. As P_{D1} and P_{D2} are coordinated in a similar manner as the chlorophylls of P700 in PSI (Jordan $et\ al.$, 2001) and the bacteriochlorophyll b of P960 in PbRC (Deisenhofer $et\ al.$, 1995) unusual coordination must be excluded. This is different for Chl_{D1} and Chl_{D2} as the central ligand for Mg^{2+} cation is not yet determined (see next chapter). The positive charge of D2-Arg180 is found to tune the high redox potential of P_{D2} (see above), whereas neither for Chl_{D1} nor for Chl_{D2} such charged residue could be identified. The calculated redox potentials of the Chl$a$ cofactors with full account of protein environment result in redox potentials of 1.14–1.21 V for P_{D1} and P_{D2}, which are as high as the redox potentials of the two accessory Chl$a$ (Acc-Chl) (Ishikita $et\ al.$,

2004). These findings could explain why the neighbouring chlorophylls Chl_{D1} and Chl_{D2} are "protected" form being oxidised by P_{D1} and P_{D2}.

6.2.2   Accessory chlorophyll *a*

Chl_{D1} and Chl_{D2} are found in positions equivalent to the two accessory bacteriochlorophyll *b* in PbRC. In contrast to PbRC, they are not coordinated by histidines, but probably by water molecules H-bonded to D1-Thr179Oγ and to the backbone oxygen of D2-Val175, respectively (Table 10.3). This coordination is similar to the situation described in PSI, where accessory chlorophyll molecules eC-A2 and eC-B2 are coordinated *via* water to the protein backbone (Jordan *et al.*, 2001). There is one notable difference as PSI eC-A2 is coordinated to the protein backbone of the B-branch and not of the A-branch. The binding pockets of Chl_{D1} and Chl_{D2} are both hydrophobic (Table 6.1) with two notable differences: first, in the Chl_{D1} binding pocket there are three Met residues but none in the Chl_{D2} pocket and second, there is only one direct H-bond in the Chl_{D2} pocket between D1-Gln199NεH and the carboxymethyl carbonyl oxygen but none in the Chl_{D1} pocket (Table 10.1).

6.2.3   Pheophytin *a*

$Pheo_{D1}$ is located between TMH-**c** of D1 and -**d** of D2 (Fig. 6.3), while $Pheo_{D2}$ between TMH-**c** of D2 and TMH-**d** of D1. $Pheo_{D2}$ is only in van der Waals contact with non-polar side chains whereas in the environment of $Pheo_{D1}$ there are some polar side chains (Table 6.1) that form three H-bonds: between D1-Gln130NεH and the keto oxygen; D1-Tyr126OηH and carboxymethyl carbonyl oxygen; D1-Tyr147OηH and carboxyphytyl carbonyl oxygen, (Table 10.1). Especially the H-bond D1-Gln130NεH to the keto oxygen, which is part of the conjugated system in the porphyrin cycle, is expected to have a major influence on the electronic structure of the $Pheo_{D1}$. Interestingly the *psbA2* gene encodes for a glutamate at D1-130 (see chapter 8.1). In *Synechocystis* sp. PCC 6803, the residue D1-Gln130 was mutated to D1-Glu130, resulting in a modified quantum yield of $P680^+Pheo^-$ (Giorgi *et al.*, 1996).

Conversely, $Pheo_{D2}$ is embedded in a strictly hydrophobic binding pocket (Table 6.1) and not in any direct H-bond to the protein matrix (Table 10.3).

In PbRC, M-Tyr208 is important for fast charge separation, and replacement by Leu208 decreases the rate of primary electron transfer (Huppman *et al.*, 2002). The analogous amino acid in PSIIcc is the conserved D2-Leu205, located in a strategic position close to Chl_{D1} at 5.3 Å, to $Pheo_{D1}$ at 3.4 Å, to P_{D1} at 4.9 Å and to P_{D2} at 4.7 Å. The exchange of Tyr by Leu might be responsible for the slower charge separation in PSII compared with PbRC (Fleming *et al.*, 1988). The complementary residue on the other branch is Phe (D1-Phe206) as in PbRC.
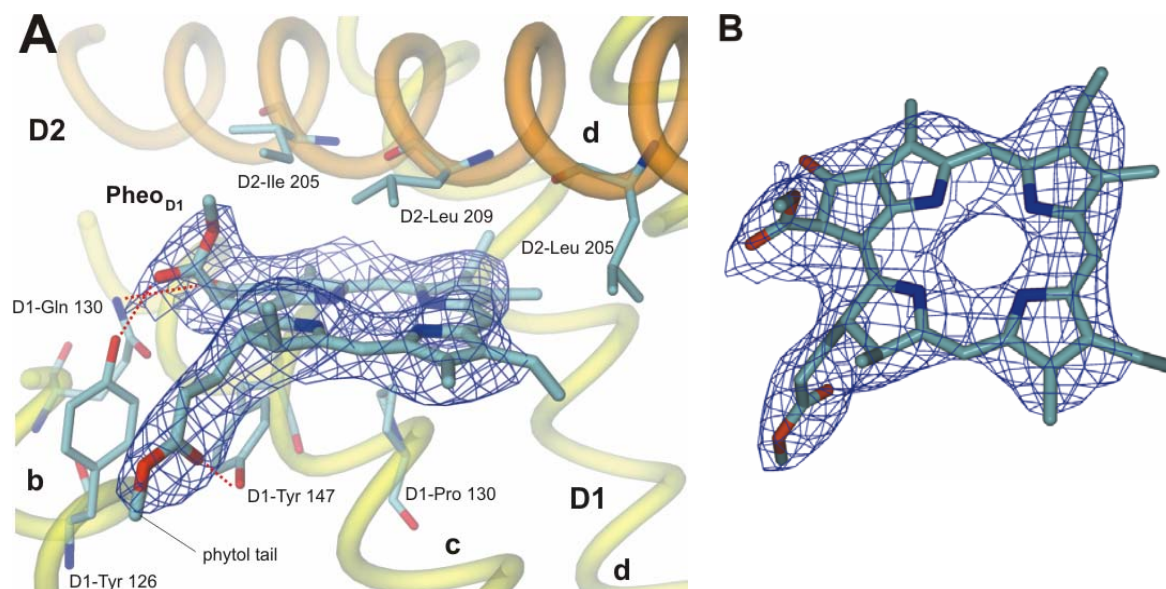

Fig. 6.3: (**A**) Environment of $Pheo_{D1}$. The cofactor is embedded within TMH **c** of D1 (yellow) and **d** of D2 (orange), respectively. Electron density (blue) is contoured at 1.2 σ level. Side chains and a fragment of the phytol chain of $Pheo_{D1}$ are clearly defined in the electron density. (**B**) $Pheo_{D1}$ and electron density (blue) is contoured at 1.2 σ level.

6.2.4 Peripheral Chlz$_{D1}$ and Chlz$_{D2}$

The contribution of the two peripheral Chl*a* to electron transfer was proposed by Michel and Deisenhofer (1988) and supported by mutational studies on D2-His117 in *Synechocystis* 6803, resulting in loss of photosynthetic growth of these cyanobacteria (Pakrasi and Vermaas, 1992). Both Chl*a* are not involved in primary charge separation and they show slow energy transfer to P680 (Schelvis *et al.*, 1994). It was suggested that the peripheral Chlz of PSII could play a central role in energy transfer from CP47 and CP43 to the ETC (Lince and Vermaas, 1998; Vasil'ev and Bruce, 2000). The first X-ray structure (Zouni *et al.*, 2001) demonstrated already that this assumption could not hold true. The orientations and positions of both Chlz molecules are not favourable for transfer to the RC (Vasil'ev *et al.*, 2001).

$Chlz_{D1}$ is at the periphery of the complex and located towards the lumenal side of the membrane between TMH-**a** and -**b** of D1, unassigned TMH **1** and part of the **ab**-loop of D1. Its Mg^{2+} is coordinated by D1-His118Nε2 (Table 10.3). Apart from this no other possible H-bonds between protein and cofactor can be deduced from the present model, although for the unassigned TMH **1** the density is not good enough to model side chains and therefore the identity of residues of this helix is not clear. The binding pocket is built up of hydrophobic residues (Table 6.1 and Table 10.3), with the exception of D1-Thr40 and D1-Gln113. Ring V of $Chlz_{D1}$ points towards the lumenal side towards the **ab**-loop of D1. The phytol chain is incompletely built and located aside of unassigned TMH **1**.

$Chlz_{D2}$ is embedded at the cytoplasmic side between TMH-**b** and -**a** of D2 and unassigned TMH **8** and **9** and the **ab**-loop of D2. Furthermore TMH-**a** of D2 and unassigned TMH **9** form a part of the binding pocket (Table 3.1 and Table 6.1). The central Mg^{2+} is coordinated by D2-His D117Nε2 (Table 10.1). The side of ring V is shielded by the **ab**-loop. Nearby D2-Thr112 is located, which could form an indirect H-bond *via* a water molecule with the methyl ester group. The other side of the binding pocket is shielded by unassigned TMH **9**, therefore no conclusion about the nature of residues on this side can be drawn at present. The only other notable residue in the pocket is D2-Cys40, whose SH-group points towards ring I (3.8 Å to the closest atom of the heterocycle). The phytol chain of $Chlz_{D2}$ points at the direction of Chl*a*21 in the antenna subunit CP47. The closest cofactor to $Chlz_{D2}$ is the Car, whose head group is in an edge to edge distance of 4.4 Å. A probable function of Car might be a role in secondary electron transfer (see chapter 6.4), when the turnover of the oxygen-evolving complex is blocked. $Chlz_{D2}$ as well as cyt *b*-559 and Car could act as alternate electron donors (Tracewell *et al.*, 2001b).

6.2.5 The non-haem Fe^{2+}

The non-haem iron is located on the local pseudo-$C2$(Fe^{2+}) axis and is coordinated by four histidines provided by the four-helix bundle formed by TMH-**d** and -**e** of D1 and D2 (Fig. 6.4A and Table 6.1). Four sequentially and structurally homolog histidines and bidentate glutamate (M232) provide the non-haem iron ligands in PbRC (Deisenhofer *et al.*, 1995). There is however, no equivalent of Glu M232 in PSII. Interestingly, D1-His215 and D2-His214 may serve dual functions. They coordinate with their unprotonated Nε to Fe^{2+}, while

Nδ-H groups could form H-bonds with Q_A and Q_B, thereby facilitating electron transfer between these groups. For a more detailed description of protein-protein interactions see chapter 4.3.1. FTIR-spectroscopy identified specific interactions of bicarbonate with the Q_B pocket. The data strongly indicated interaction of bicarbonate with D1-His215 of the Q_B pocket either directly or *via* a hydrogen bond network. The properties of bicarbonate could explain the specific properties of the quinone-iron electron acceptor side in PSII (Govindjee and Van Rensen, 1993). It has a strong influence on the electron transfer rates between the quinones (van Rensen, 2002) and influences the midpoint potential of the non-haem iron.
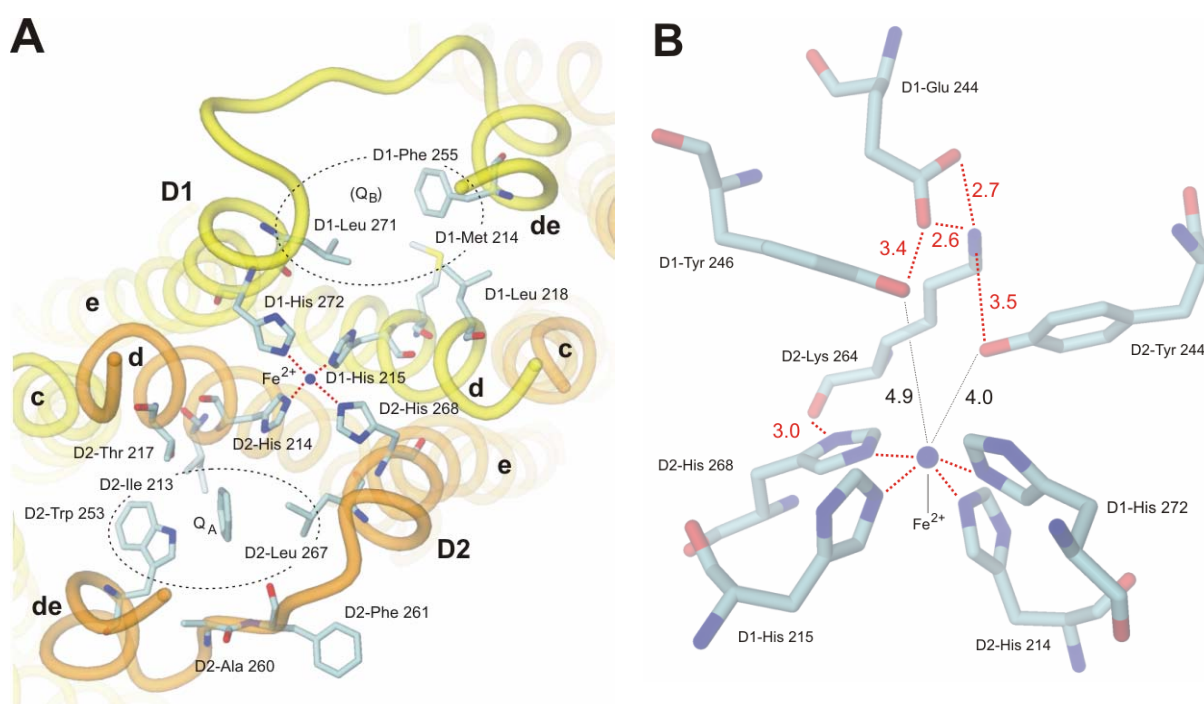

Fig. 6.4: Quinone binding sites and non-haem Fe^{2+}. (**A**) The cytoplasmic side of the D1/D2 heterodimer with non-haem iron and quinone binding pockets. The view is onto the membrane plane from the cytoplasmic side. D1 and D2 are shown in yellow and orange, helices are labeled as in Fig 2. The binding pockets for Q_A and Q_B are indicated, and amino acids forming the binding pockets are shown. (**B**) Coordination of the non-haem Fe^{2+}. Dashed red lines indicate H-bonds. The black line gives the direct distance of the phenolic oxygens to the Fe^{2+}. All distances are given in Å.

On the cytoplasmic side, Fe^{2+} could be indirectly coordinated by OηH groups of D1-Tyr246 and D2-Tyr244 appearing at 4 to 5 Å distance to Fe^{2+} (Fig. 6.4B), suggesting that a water molecule or possibly bicarbonate mediates the interaction (Berthomieu and Hienerwadel, 2001) but the electron density is too poor to allow a decisive interpretation.

The electron transfer chain

The two Tyr residues themselves are stabilised by long H-bonds (3.4 and 3.5 Å) provided by D1-Glu144 and D2-Lys264 (Fig. 6.4B and Table 10.1). The H-bonding network shown in Fig. 6.4 suggests that D2-Lys264 plays in important role in the stabilisation of the non-haem Fe^{2+} site. The backbone oxygen stabilises D2-His268 and the side chain is involved in H-bonding on the cytoplasmic side. This arrangement contrast the structure of Ferreira *et al.* (2004), where D2-Lys264 interacts directly with bicarbonate, instead of D2-Tyr244.

At the D1/D2 interface formed by TMH-**d** of both subunits, D1-Cys212 and D2-Cys211 appear to be involved in inter-subunit interaction by forming a weak H-bond or even a disulfide bridge upon oxidation (Fig. 4.5). D2-Cys211 is highly conserved, while D1-Cys212 is limited to *T. elongatus* and replaced by Ser or Ala in other known D1 sequences (see chapter 4.3.1 and 8.1).

6.2.6   The primary quinone - Q_A

The primary electron acceptor Q_A in PSIIcc is a plastoquinone (PQ) tightly bound to D2. On the cytoplasmic side, Q_A is shielded by the surface helix **de(1)** of D2 (from D2-Thr243 to D2-Ser254) and the loop region between **de(1)** and TMH-**e** (D2-Gln255 to D2-Asn263). On both sides the binding pocket is flanked by the C-terminal part of TMH-**d** (D2-Leu210 to D2-Asn220) and the N-terminal part of TMH-**e** (D2Lys264 to D2-Phe270). Residues of D2 forming the pocket are Ile213, His214, Thr217, Met246, Trp253, Ala260, Phe261, Leu267 (Fig. 6.4A and Table 6.1). The quinone ring of Q_A is sandwiched between D2-Leu267 and D2-Trp253 but the ring plane is not parallel to the indol ring of D2-Trp253, resulting in reduced π-stacking. This is in contrast to PbRC of *Blastochloris viridis* where the indol ring of TrpM252 is roughly parallel to the ring of the primary quinone. Possible H-bonding donors for interaction with the keto oxygens of Q_A would be D2-His214Nε, D2-Thr217Oγ, D2-Trp253Nε and/or D2-Phe261NH but as the keto oxygens of the Q_A can not be modelled at the present resolution, no definite statement about H-bonding interactions is possible. In the 3.5 Å resolution structure Q_A is modelled with H-bonding interactions to D2-Phe261O (Ferreira *et al.*, 2004).

The centre-to-centre distance between Q_A and $Pheo_{D1}$ is 13.9 Å. Between the Q_A-pocket and the fifth ring of $Pheo_{D1}$ residues D2-Ile213 and D2-Trp253 are found. The indol side chain of D2-Trp253 could function as bridge between Q_A and $Pheo_{D1}$ as its Nε is close to Q_A and its aromatic ring is at 5 Å to the $Pheo_{D1}$ keto oxygen. D2-Trp253 is conserved from

cyanobacteria to higher plants as is D2-Phe252, which might influence the aromatic system of D2-Trp253. Another H-bond to the quinone-carbonyl is provided in PbRC by M-Thr220OG, which corresponds to D2-Thr217 in PSII. The sequence between the coordinating D2-His214 and D2-217 is conserved from cyanobacteria to higher plants. The non-haem iron is 9.0 Å away from the Q_A ring (Fig. 6.1 and Table 10.2) and the two histidines D2-His214 and D2-His268 as well as D2-Leu267 lie between them (Fig. 6.4).

An elongated patch of electron density is visible in the vicinity of Q_A that is not yet assigned to any special feature. This elongated density might be interpreted as isoprenoid chain of Q_A beside other possible interpretations (acyl chain of a lipid, detergent or part of a carotenoid). If we would assume that this density belongs to the Q_A this would imply a conformation of the tail not in agreement with the 3.5 Å structure (Ferreira *et al.*, 2004).

6.2.7   The secondary quinone - Q_B

The charge on Q_A^- is passed to another plastoquinone, referred to as Q_B. After two photosynthetic cycles doubly reduced plastoquinone is protonated and plastoquinol is released from its binding niche in D1 to the plastoquinone pool in the thylakoid membrane and an oxidised plastoquinone takes its place. Plastoquinols from this pool supply electrons to the cyt b_6f complex.

The overall structure of the Q_B binding site is shown in Fig. 6.4. The Q_B site is formed exclusively by D1, in more detail by the C-terminal part of TMH-**d** (D1-Gly207 to D1-Val219), the cytoplasmic surface helices **de(1)** and **de(2)** and the loop region connecting them as well as the N-terminal part of TMH-**e** (D1-Arg269 to D1-Phe274) (Fig. 6.4 and Table 6.1). Residues in the binding pocket include Phe211, Met214, His215, Leu218, Ala251, Phe255, Ile259, Leu271 and Phe274, all from D1. As no electron density for PQ9 was found, no conclusions about possible H-bond interactions can be drawn at present.

Inspection of the Q_B-pocket revealed no electron density at an position corresponding to the Q_B molecule in PbRC (Stowell *et al.*, 1997). In PSIIcc the quality of the electron density maps around the Q_B pocket is weakly defined, indicating a high flexibility of this region. This is similar to the 3.8 Å resolution structure (Zouni *et al.*, 2001) and is in agreement with the observations in the 3.7 Å resolution structure (Kamiya and Shen, 2003) but in contrast to the

The electron transfer chain

3.5 Å structure (Ferreira *et al.*, 2004), where a PQ9 was placed in a position similar to the proximal position of Q_B in PbRC (Stowell *et al.*, 1997).

Our observations are in line with the findings in PbRC structures. In the first PbRC structure at 3.0 Å resolution from *B. viridis* menaquinone was found in the Q_A side, but the Q_B site was not occupied and could only be mapped by measuring crystals soaked with ubiquinone analogs and Q_B site inhibitors (Deisenhofer *et al.*, 1985).

In the various structures from the PbRC of *Rhodobacter sphaeroides* and *B. viridis* the region of the Q_B site is the least well defined one, revealing large deviations between the different structures for the position of the Q_B. The atomic displacement factor of Q_B (25.5 $Å^2$) is greater than of Q_A (12.0 $Å^2$) (Deisenhofer *et al.*, 1995). The high atomic displacement factor of Q_B compared to the average atomic displacement factor for the polypeptide (21.7 $Å^2$) suggests that the binding site is only partly occupied or has a higher degree of flexibility. The occupancy of the Q_B pocket in PbRC crystals from *B. viridis* was estimated to be only ~30% (Deisenhofer *et al.*, 1995). Due to the poor quality of the electron density modelling of the ubiquinone in the Q_B site is strongly dependent on the positioning of the isoprenoid chain. As the region of the isoprenoid chain is close to the surface of the protein where the electron density is less well defined a differentiation between detergent molecules, lipids or the isoprenoid chain is difficult. Only with higher resolution structures (around 2.5 Å) modelling of these regions improved and revealed the presence of a lipid, occupying part of the electron density ascribed to the isoprenoid chain of ubiquinone in previous models (Camara-Artigas *et al.*, 2002). For PSIIcc it is not unexpected to find no density in this site at the present resolution, as we have in our preparations a maximum occupancy of 50% of the Q_B site (see above). The Q_B binding pocket in PSII is less buried compared to the PbRC, where the H-subunit covers the cytoplasmic side of the L-subunit. This in turn implies a higher solvent accessibility in PSII associated with an easier loss of the quinole and lowering its occupancy. In addition the hydrophobic tail of lipids or detergent molecules, mimicking the phytol chain of a quinone could more easily compete with for the hydrophobic pocket. Differences in herbicide binding between PSII and PbRC imply a possibly different architecture of the Q_B binding pocket in PSII (Oettmeier, 1999).

All these mentioned aspects are hampering the elucidation of the Q_B binding pocket. Another aspect is the condition of illumination; the exposure to X-ray radiation or light may lead to

charge separation and partial formation of reduced secondary quinone. This formation of Q_B^- might be coupled to structural changes (Reifarth and Renger, 1998) as observed in light and dark state structures from PbRC (Stowell *et al.*, 1997; Fritzsch *et al.*, 2002) that increase the disorder at this site.

6.2.8 Tyr$_Z$

The electrochemical midpoint potential (E_m) of neutral tyrosine radicals is one of the least oxidising among all amino acids and therefore the protein environment is protected from being oxidised. The different redox chemistry of Tyr$_Z$ and Tyr$_D$ must be reflected by differences in the protein environment. According to $^2H_2O/^1H_2O$ exchange studies (Ahlbrink *et al.*, 1998; Diner *et al.*, 1998; Tommos and Babcock, 1998), Tyr$_Z$ is solvent accessible and is in a more hydrophilic environment compared to Tyr$_D$ (Fig. 6.5 and Table 6.1).
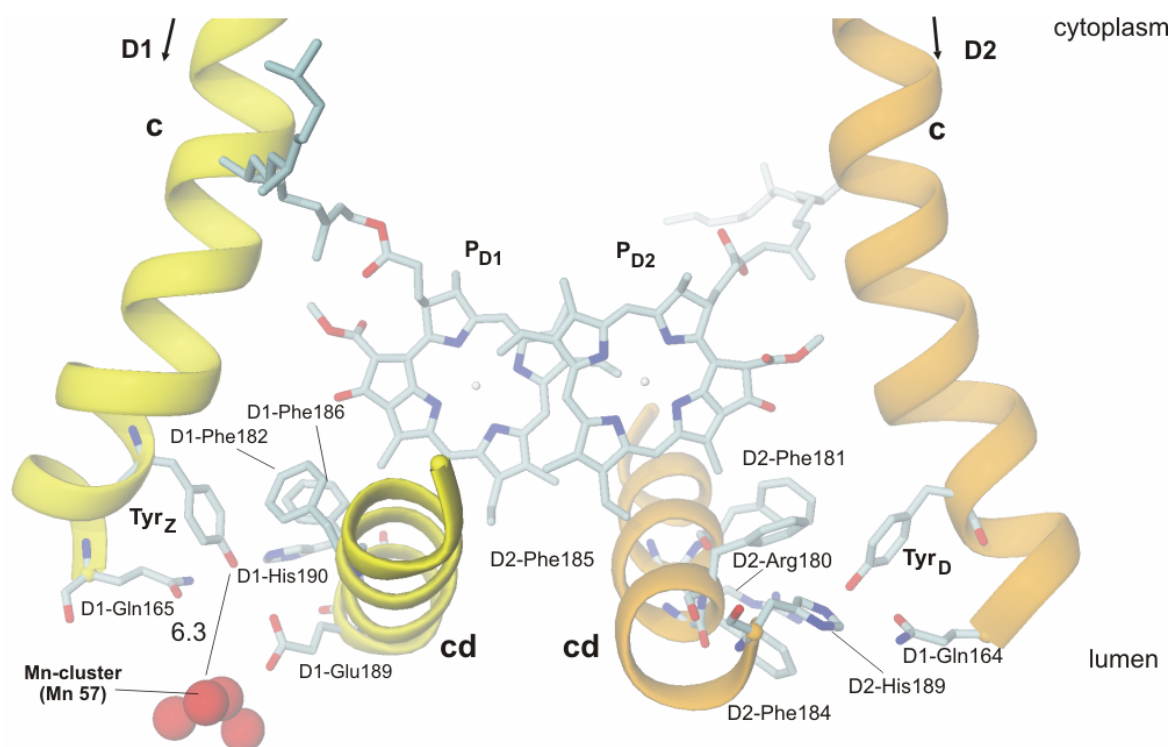

Fig. 6.5: The environment of Tyr$_Z$ and Tyr$_D$. Tyr$_Z$ is embedded in D1 (yellow) and Tyr$_D$ in D2 (orange). The Mn-Ca-cluster is indicated by red spheres and P_{D1}/P_{D2} are shown as stick models in grey. The distance between Mn(57) and Tyr$_Z$ is given in Å.

There are only the two bulky side chains D1-Phe182 and D1-Phe186 in the binding pocket of Tyr$_Z$ located on helix **cd** (Fig. 6.6), both in close proximity to P_{D1} (Table 6.1). EPR

investigations revealed a distance of 7.9 Å between Tyr_Z and the Mn-Ca-Cluster (Lakshmi *et al.*, 1999). The conserved D1-Phe186 seems to have a strategic position modulating the spatial arrangement and redox properties as shown in mutation studies of *Synechocystis* (Wiklund *et al.*, 2001). The phenolic $Tyr_ZO\eta$ is H-bonded to D1-Glu189Oϵ, to D1-Gln165Oϵ/Nϵ and to D1-His190Nϵ. The position of the imidazol ring of D1-His190Nϵ is fixed by an additional H-bond to D1-Asp298. The interactions of $Tyr_ZO_\eta H$ with D1-His190Nϵ and D1-Glu189Oϵ agree with the assumption that Tyr_Z has to be deprotonated prior to oxidation to $Tyr_Z^{\bullet+}$ (Mamedov *et al.*, 1998; Hays *et al.*, 1999). Siegbahn and coworkers tried to calculate the redox-potential of Tyr_Z and reported that only the presence of negatively charged carboxylate allow to describe the native system (Siegbahn and Blomberg, 2004). This is in good agreement with the close vicinity of D1-Glu189.
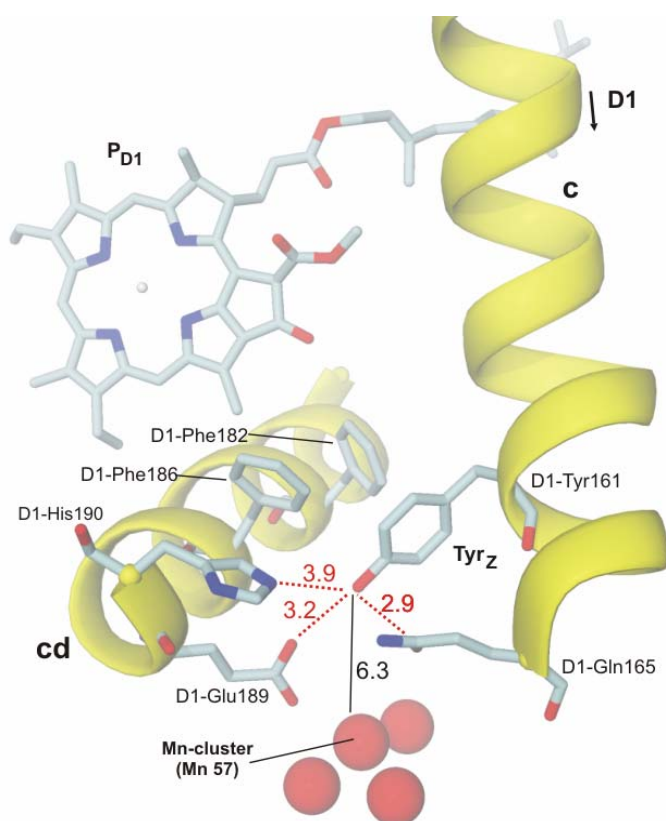

Fig. 6.6: Tyr_Z is embedded in D1 (yellow). The Mn-Ca-cluster is indicated by red spheres and P_{D1} is shown in grey. Possible H-bonding distances are given in Å. Tyr_Z is involved in H-bonding (red dotted lines).

The Mn-Ca-cluster and phenolic $Tyr_ZO\eta H$ (D1-Tyr161OηH) are bridged by the carboxylate of D1-Glu189 (Fig. 6.6). $Tyr_ZO\eta H$ is separated by 13 Å from the central Mg^{2+} of P_{D1} (Table 6.1 and Table 10.2) and closest edge-to-edge distance of 6.9 Å.

The high redox potential of P680 provides the driving force for oxidation of water. This unique high redox potential could also damage the surrounding protein matrix. Therefore an ETC with precise control of redox-potential and reorganisation energy is required. A large fraction of $P680^+$ is reduced by Tyr_Z in nanoseconds (20–40 ns for S_0, S_1; 50–250 ns for S_3, S_4) but slower phases also occur (Jeans *et al.*, 2002). A leading model is the hydrogen-abstraction-model developed by Babcock and collaborators (Tommos and Babcock, 1998; Debus *et al.*, 2000; Tommos and Babcock, 2000; Pace and Ahrling, 2004). In this model and subsequently modified forms, $Tyr_Z^\bullet$ is an abstractor of hydrogen atoms from the Mn-Ca-cluster on each turnover. Charge distribution onto a hydrogen-bonding network leading to proton release is proposed to start at D1-His190, which accepts the proton from Tyr_Z. D1-His190 next to D1-Glu189 is located close to the Mn-Ca-cluster and, according to mutation studies, could participate in a H-bond network that modulates the properties of both, Tyr_Z and Mn cluster.

6.2.9 Tyr_D

Several functions have been proposed for Tyr_D, some of them are supported by experimental evidence. First it was demonstrated that Tyr_D can oxidise the Mn-Ca-cluster from the S_0 state to the S_1 state and would therefore be important for the stability of the cluster in the dark and during photoactivation (Vermaas *et al.*, 1988). It has recently been shown experimentally that the absence of Tyr_D indeed affects photoactivation (and the yield of oxygen evolution) (Ananyev *et al.*, 2002). This indirect electrostatic effect of $Tyr_D^\bullet$ could restrict the chlorophyll cation to P_{D1} and this could be important in terms of D1 turnover, making sure that the most oxidizing species (and hence oxidizing damage) is limited to D1. Tyr_D (D2-Tyr160) is 35 Å from Tyr_Z as predicted by pulsed EPR on plant protein (Astashkin *et al.*, 1994). This is in good agreement with a distance ($Tyr_ZO\eta$ to $Tyr_DO\eta$) of 28.7 Å determined with our coordinates (Table 10.2).
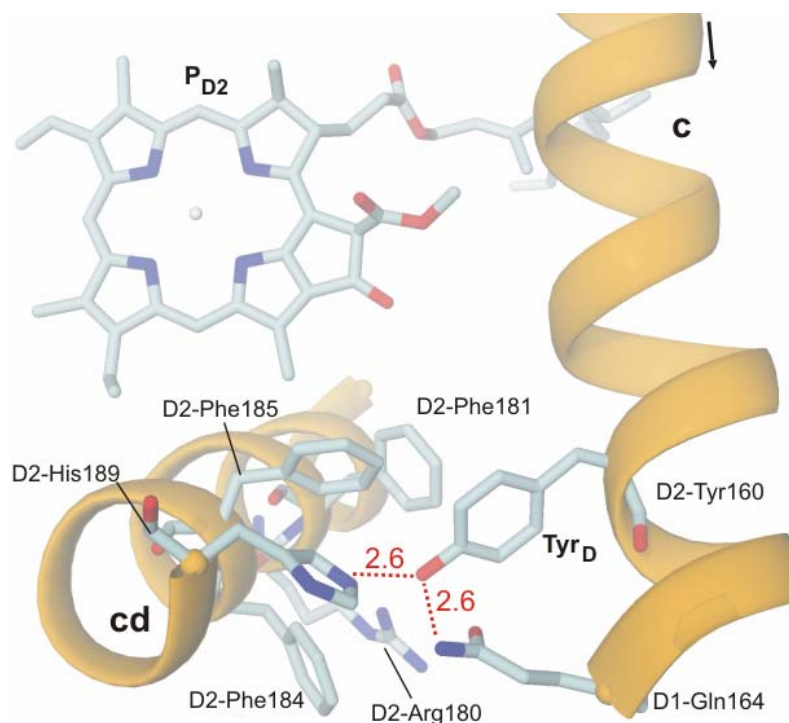
The electron transfer chain

Fig. 6.7: Tyr_D is embedded in D2 (orange). P_{D2} is shown in grey. Possible H-bonding distances are given in Å. Tyr_D is involved in H-bonding (red dotted lines).

Tyr_D is symmetry related to Tyr_Z located on the hydrophobic side of helix **cd** and found in a predominantly hydrophobic environment, formed by the aromatic side chains of D2-Phe181, D2-Phe184 and D2-Phe185, (Table 6.1). Helix **cd** is placed between Tyr_D and P_{D2} and the residues D2-Phe181 and D2-Phe185 and bridges both cofactors (Fig. 6.5 and Fig. 6.7). Additional bulky side chains are D1-Phe169 and CP47-Phe362. The only hydrophilic residues in the binding pocket are polar D2-Gln164 and D2-His189. Tyr_DOηH forms two short H-bond to D2-Gln164 (2.6 Å) and to Nε of D2-His189 (2.6 Å) (Table 10.1). The latter short H-bond was predicted by spectroscopy (Campbell *et al.*, 1997; Diner *et al.*, 1998) and is in very good agreement with our structural model. The Nδ-H group of D2-His189 is stabilised by an H-bond to the backbone oxygen of D2-Arg294, leading to an H-bond network.

6.2.10 The oxygen evolving centre

The oxygen evolving centre (OEC) is the catalytically active site of PSII, composed of four Mn cations and Ca^{2+} as well as one chloride anion. In one reaction cycle two water molecules are split to oxygen and protons. After four single flashes, one molecule of oxygen evolves with a peculiar oscillatory pattern. The third flash results in the maximum oxygen yield.

Thereafter, the amount of oxygen produced peaks with every fourth flash until the oscillation damps out to a steady state. Concluding, the OEC must undergo four light-dependent reactions before the release of oxygen (Fig. 6.8).
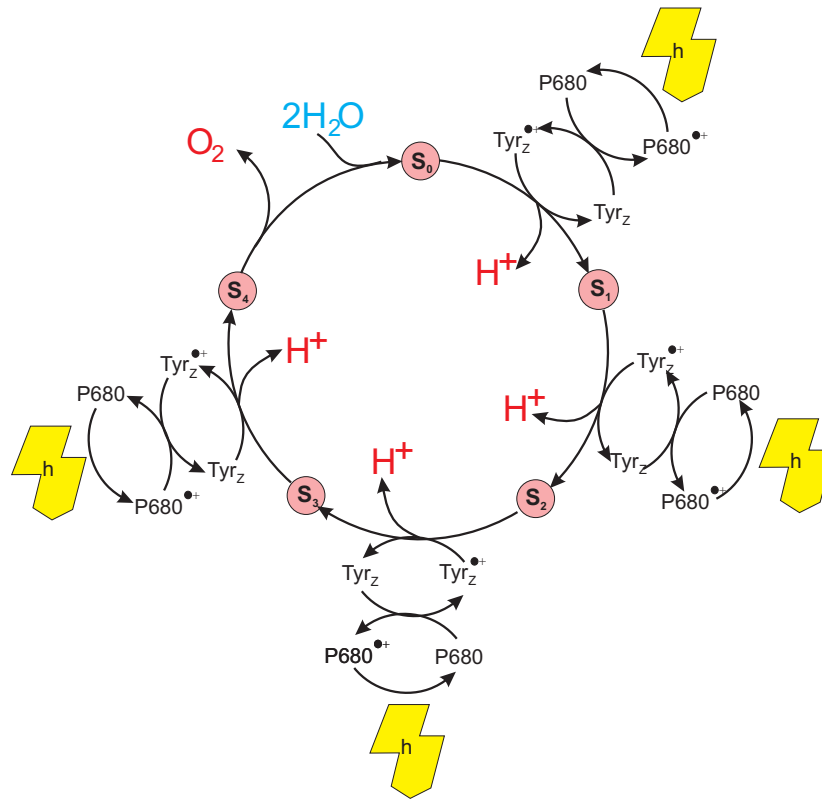

Fig. 6.8: The Kok-cycle: yellow flashes indicate the four light flashes needed for water oxidation. The five S_i-states are indicated as pink circles. The educt is water (blue), whereas the products are molecular oxygen and protons (red).

The OEC cycles through five different states, named S_0 to S_4. Oxygen is released between the S_4 and S_0 cycle (Kok *et al.*, 1970). During the S-cycles, the Mn cations change their redox states. S_1 seems to be the most stable state as oxygen is first released at the third and thereafter at the fourth flash. During water oxidation a total of four protons are released to the lumen since the E_m of O_2/H_2O was measured to be 0.815 V, the five S-states have to have a very high redox-potential. Furthermore the OEC has to stabilise highly reactive intermediates in an aqueous environment.
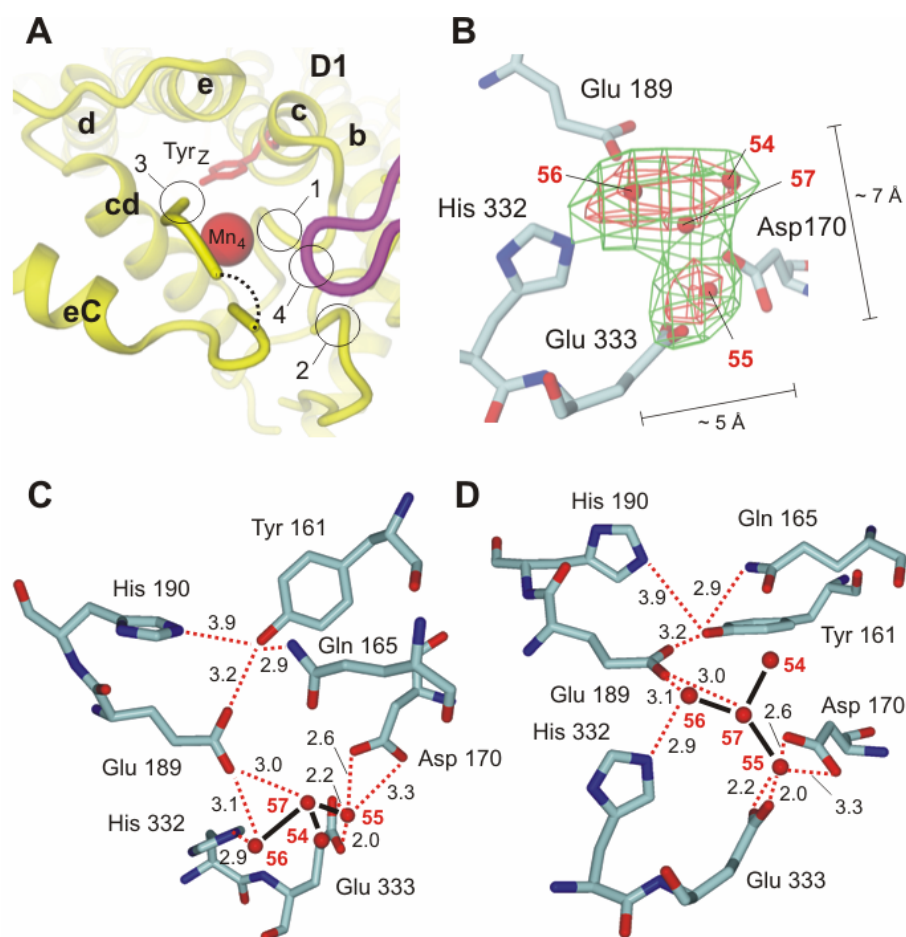
The electron transfer chain

Fig. 6.9: Protein environment and coordination of Mn-Ca-cluster and Tyr$_Z$. (A) Location of the Mn-Ca-cluster, view from the lumen. Important structural elements in D1: TMH-**c**, lumenal helices **cd** and **eC**, loops **c-cd** (1), **a-ab** (2) and C-terminus (3); in CP43: loop **ef(2)-f** (4, magenta). Dotted black line shows connection of D1 downstream **eC**. (B) Electron density around Mn-Ca-cluster contoured at two levels: 3.5 σ (green) for the shape of Mn-Ca-cluster and 5.3 σ (red) for the two high electron density peaks, view from the lumen. (C and D) Interactions in the region of Mn-Ca-cluster and Tyr$_Z$ in two perpendicular views rotated about the horizontal. Black bold lines indicate closest connections between Mn ions. H-bonding and coordinating distances in Å (red dotted lines). Side chains belong to D1, TMH-**c** (Tyr161, Gln165), loop **c-cd** (Asp170), helix **cd** (Glu189, His190) and helix **eC** (His332, Glu333). Other possible ligands from the loops **a-ab** in D1 and **ef(2)-f** in CP43 were not clearly visible in the electron density.

The cluster of 4 Mn cations is located at the lumenal side of D1 and surrounded mostly by residues from this subunit and by some (not modelled) side chains from CP43 (Fig. 6.9). Its electron density contoured at 3.5 σ level is Y-shaped with dimensions 5 x 7 x 3 Å (Fig. 6.9). This changes at the 5.5 σ level to two distinct peaks, one larger and the other smaller harbouring probably 3 and 1 Mn cations, respectively. Our X-ray diffraction data measured at and beyond the Mn-edge confirm the presence of Ca^{2+} near the larger density peak of Mn,

making interpretation in terms of a Mn-Ca-cluster possible. From this data the most probable of the four ions, which might be Ca^{2+}, is Mn57 (Fig. 6.9). Assuming that all four cations are Mn would be in agreement with the 3+1 model structures derived from EPR and EXAFS data (Carrell *et al.*, 2002).

EXAFS at the Mn absorption edge is used to study the local structure of the Mn cations and proposed topologically consistent models that can be reconciled with several structural arrangements of the four Mn atoms (DeRose *et al.*, 1994). EPR studies indicate that the four Mn cations are arranged in a structure with three strongly exchange-coupled Mn cations that are coupled more weakly to the fourth Mn. The proposed model consists of two or three di-μ-oxo-bridged binuclear Mn units with strongly coupled Mn–Mn distances of about 2.7 Å that are linked to each other by a mono-μ-oxo bridge with a Mn–Mn separation of about 3.3 Å, and with Ca^{2+} at a distance of 3.4 Å to Mn (Yachandra *et al.*, 1993; DeRose *et al.*, 1994; Cinco *et al.*, 2004). The Mn–Mn distances are largely invariant in the native S_1 and S_2 states (DeRose *et al.*, 1994). EXAFS experiments on the S_3 and S_0 states have been difficult to perform on PSII samples using single flashes. Ca^{2+} and chloride are the necessary cofactors for the proper function of the OEC of PSII (Debus, 1992). While the Mn complex has been extensively studied by X-ray absorption techniques (XANES and EXAFS), comparatively less is known about the Ca^{2+} cofactor. The fewer number of studies on the Ca^{2+} cofactor have sometimes relied on substituting the native cofactor with Sr^{2+} or other metals (Ghanotakis *et al.*, 1985; Boussac and Rutherford, 1996) and have stirred some debate about the structure of the binding site. Sr^{2+} has a similar ionic radius as Ca^{2+} as well as a pK_a of its aqua ion that is close to that of Ca^{2+} and therefore can functionally substitute for Ca^{2+}. Efforts using Mn EXAFS on Sr^{2+} substituted PSII (Latimer *et al.*, 1995) and Sr^{2+} EXAFS (Cinco *et al.*, 1998; Cinco *et al.*, 2004) have indicated a close link between the Mn cluster and Sr^{2+}, within 3.5 Å. Nevertheless, other experiments have given contradicting results (Riggs-Gelasco *et al.*, 1996).

The two models of OEC (Fig. 6.9) agree in terms of having two moieties: one smaller containing one cation and one larger containing three or more cations. The exact positions and identity of the cations are affected by insufficient quality of data and different approaches in the interpretation of electron density. Obviously, higher resolution (< 2.9 Å) data are necessary to complete a reliable model of the OEC, as the EXAFS- derived Mn-Mn distance is about 2.9 Å (Robblee *et al.*, 2001). The side chains of D1-Asp170, D1-Glu189, D1-His332 and D1-Glu333 are close enough for direct coordination of Mn cations (Fig. 6.9 and Table
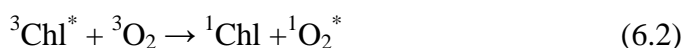
10.1), in agreement with mutation studies (Debus, 2001; Diner, 2001). Additional coordination could be provided by residues located in the loop **a-ab** and in the C-terminal region of D1, which are not clearly defined in the electron density. According to biochemical data the likely ligands would be D1-His337, D1-Asp342, D1-Ala344 (Debus, 2001; Diner, 2001). Most of the protein ligands are in agreement with the recent 3.5 Å resolution structure (Ferreira *et al.*, 2004). CP43-Glu354 proposed to coordinate Mn in (Ferreira *et al.*, 2004) is close to the cluster but its side chain is not visible in our electron density (see chapter 4.4.2).

6.3 Carotenoid

Besides the chlorophyll molecules of the antenna system and reaction centre, *β*-carotenes are the second frequently occurring pigment within PSII. Carotenoids fulfil a diverse set of functions in PSII (Frank and Brudvig, 2004): since the carotenoids absorb light at a wavelength range of 450 nm to 570 nm, they function as additional pigments to harvest sunlight filling the spectral gap of chlorophyll molecules, leading to a higher efficiency of the whole system. Having absorbed a photon, the energy is transferred to Chl*a* according to:

$$^1Car^* + Chl \rightarrow Car + {}^1Chl^* \qquad (6.1)$$

Furthermore carotenoids protect PSII from photo-oxidation. Since both processes underlie the energy transfer, *β*-carotenes should be close to neighbouring chlorophyll molecules (according to the Dexter theory).

$$^3Chl^* + {}^3O_2 \rightarrow {}^1Chl + {}^1O_2{}^* \qquad (6.2)$$

The protection function of the carotenes for photo-oxidation relies on their low triplet state T_0. If due to inter-system crossing a chlorophyll does not occur in an excited singlet state but in a triplet state, there is the possibility that according to eq. 6.2 singlet oxygen ($^1O_2$) is formed. Singlet oxygen is extremely toxic for the cell; therefore all organisms evaluated protection mechanisms (eq. 6.3).

$$^3Chl^* + Car \rightarrow Chl + {}^3Car^* \qquad (6.3)$$

In *β*-carotenes the triplet state T_0 is energetically below the singlet state of molecular oxygen. If the excitation energy is being transferred from a chlorophyll molecule to a *β*-carotene, the energy transfer from a carotene to molecular oxygen analogous to equitation eq. 6.3 is impossible, because the energy is not sufficient. The carotene dissipates the energy in form to heat to its environment.

Recently, Roszak and co-workers (Roszak *et al.*, 2004) gave insight into the mechanism of carotenoid binding and showed that carotenoids could stabilise protein structures. In addition it seems that Car are involved in the packing process of, at least, the TMH of D1 and D2 (Tracewell *et al.*, 2001b).

HPLC analysis of extracted carotenoids revealed that the PSIIcc from *Synechocystis* PCC 6803 contains ~17 Car molecules, of which ~14 are *β*-carotene and the rest are mainly zeaxanthin (Tracewell *et al.*, 2001a; Tracewell *et al.*, 2001b). The D1-D2-cyt *b*-559 RC complex has been found to contain two *β*-carotenes (Gounaris *et al.*, 1990). From the UV-Vis spectra of the acetone extract of *T. elongatus* the carotenoid to Chl*a* ratio of monomeric and dimeric PSIIcc was determined to be 0.255 ± 0.03 Car/Chl*a* for the dimeric PSIIcc, giving a total of 9 to 10 Car per 36 Chl*a* (Kern *et al.*, 2004a).

Carotenoids are involved in secondary electron transfer *via* cyt *b*-559 and in quenching of singlet oxygen. The latter, produced from triplet state ^{3}P680, is suggested to participate in the degradation of protein D1 (Ke, 2001). In the electron density, one all-*trans* *β*-carotene (Car_{D2}) was identified in D2 nearly parallel to the membrane plane (Lakshmi *et al.*, 2003) (Fig. 6.10). In the crystal structure of *T. vulcanus* (Kamiya and Shen, 2003) two *β*-carotenes have been identified in positions that are different from the one found here.

Car_{D2} is approximately 27 Å in length and has all-*trans* configuration. It is slightly bended and twisted. The isoprenoid chain of Car_{D2} is in van der Waals contact to hydrophobic side chains of TMH-**a** of D2 and β-chain of cyt *b*-559 (D2-Gly46, D2-Leu49, β-Phe33, β-Pro29, β-Leu34, β-Ile37), at 14.0 Å to Chl_{D2} and at 15.2 Å to the haem Fe^{2+} of cyt *b*-559 (Fig. 6.10). One jonon head group is close (4.4 Å) to $Chlz_{D2}$ surrounded by D2-Leu43, D2-Leu110, D2-Phe113 and the other jonon ring points towards the unassigned TMH **6** and is at 9.9 Å edge-to-edge distance to Chl_{D2} (Fig. 6.10).
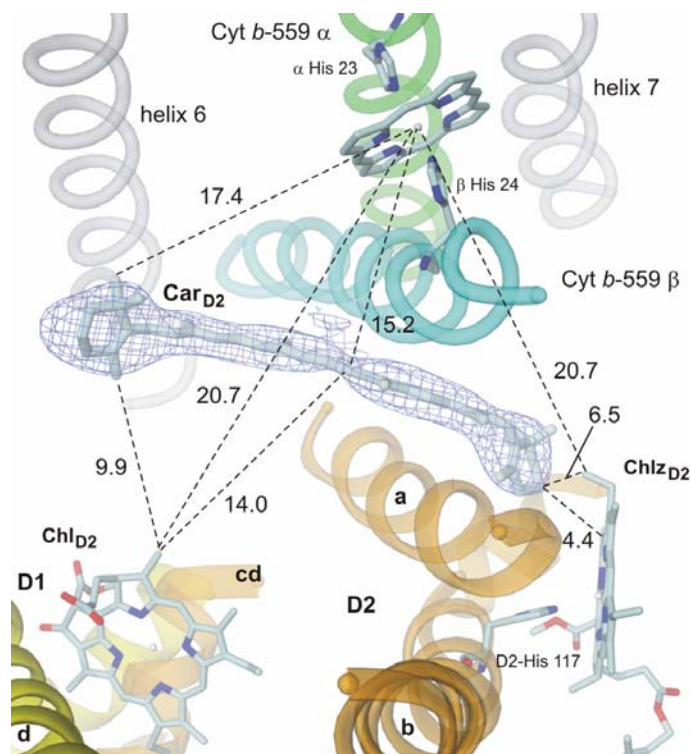
The electron transfer chain

Fig. 6.10: Location of Car_{D2} molecule in the PSIIcc complex, view onto the membrane plane from the cytoplasmic side. All distances are given in Å.

The centre-to-centre distance from Car_{D2} to non-haem Fe^{2+} is 35.7 Å, consistent with 38 Å derived from EPR spectra (Lakshmi *et al.*, 2003). The protein matrix around Car_{D2} is mainly hydrophobic. Car_{D2} could represent the *β*-carotene suggested to be involved in secondary electron transfer pathway *via* the haem of cyt *b*-559 and/or $Chlz_{D2}$ (Faller *et al.*, 2001; Tracewell and Brudvig, 2003) and corresponds to the spectroscopically identified Car_{507} (Telfer, 2002).

6.4 Secondary/cyclic electron transfer

Under conditions when the primary electron donors of PSII are inhibited, such as in Mn-depleted PSII, or at low temperatures when turnover of the oxygen-evolving complex is blocked, alternate electron donors, including cyt *b*-559, accessory chlorophylls, and *β*-carotenes, can be photo-oxidised (Tracewell *et al.*, 2001b). If not transferred rapidly to the oxygen-evolving complex, $P680^+$ can cause oxidative damage to PSII. This is a unique problem for PSII due to the high oxidation potential of $P680^+$ which can cause oxidation of its own chlorophyll and carotenoid molecules. To protect the system from oxidative damage, cyt *b*-559 is able to be photo-reduced by accepting electrons from Q_B (Buser *et al.*, 1990) or

photo-oxidised by donating electrons to $P680^+$ (Buser *et al.*, 1992). Therefore, cyt *b*-559 can participate in a cyclic electron transfer pathway within PSII.

In addition, the secondary electron transfer reactions generate Chl*a* cation radicals that are potent quenchers of excitation energy (Schweitzer and Brudvig, 1997). It has been proposed that cyclic electron transfer processes and/or quenching by Chl*a* cation radicals play a role under high-light or other stress conditions to protect the PSII reaction centre from oxidative damage (Stewart and Brudvig, 1998). Efficient electron transfer from cyt *b*-559 to $P680^+$ is hampered by the long distance of 40 Å to P_{D1} and 45 Å to P_{D2}. Car appear to act like electron wires due to their extended π-electron conjugation in the photo-oxidation of cyt *b*-559. However, the pathway(s) of electron transfer involving cyt *b*-559, Chl*a*, and Car are still unclear and pathways from cyt *b*-559 to $P680^+$ have been proposed. It is possible that the secondary electron transfer pathways include Chl*a* molecules in CP43, which could provide a novel pathway for hole migration to Chl_{ZD1} (Vasil'ev *et al.*, 2003). It should be noted that this pathway includes an additional Chl*a* in CP43 found in the *T. vulcanus* structure (Kamiya and Shen, 2003). A chain-like arrangement of Chl*a* molecules in CP43 involved in hole migration from $P680^+$ to $Chlz_{D1}$ was suggested (Vasil'ev *et al.*, 2003; Vasil'ev and Bruce, 2004). As this additional Chl*a* in the structure of Kamiya and Shen (Kamiya and Shen, 2003) as well as Ferreira *et al.* (2004) is not present in our model, we can not support this hypothesis.

It should be noted that that the plant and cyanobacterial systems developed different photoprotection mechanisms. In higher plants, the xanthophyll cycle plays an important role in photoprotection (Niyogi, 1999), but this cycle is absent in cyanobacteria.